

Document downloaded from:

<http://hdl.handle.net/10251/50883>

This paper must be cited as:

Martinez Franco, R.; Moliner Marin, M.; Concepción Heydorn, P.; Thogersen, JR.; Corma Canós, A. (2014). Synthesis, characterization and reactivity of high hydrothermally stable Cu-SAPO-34 materials prepared by one-pot processes. *Journal of Catalysis*. 314:73-82. doi:10.1016/j.jcat.2014.03.018.



The final publication is available at

Copyright Elsevier

**Synthesis, characterization and reactivity of high hydrothermally stable Cu-SAPO-34  
materials prepared by “one-pot” processes**

Raquel Martínez-Franco<sup>1</sup>, Manuel Moliner<sup>1\*</sup>, Patricia Concepcion,<sup>1</sup> Joakim R.  
Thogersen<sup>2</sup>, Avelino Corma<sup>1\*</sup>

<sup>1</sup> Instituto de Tecnología Química (UPV-CSIC), Universidad Politécnica de Valencia,  
Consejo Superior de Investigaciones Científicas, Valencia, 46022, Spain

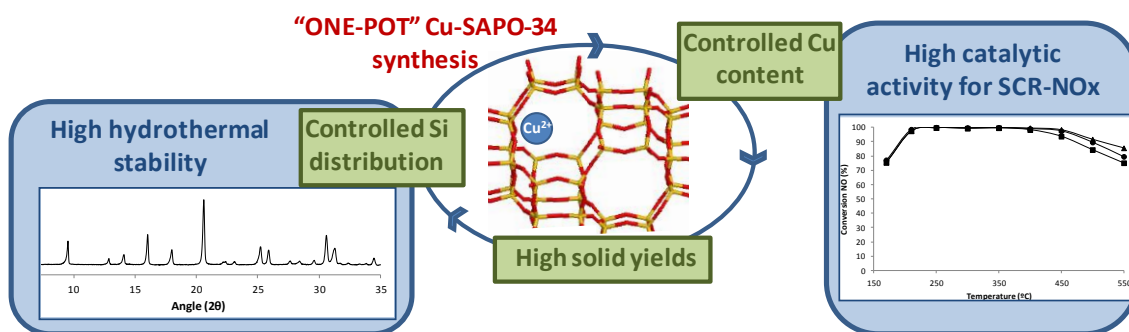
<sup>2</sup> Haldor Topsøe A/S, Nymøllevej 55, DK-2800 Lyngby, Denmark

\*Corresponding authors: E-mail addresses: [acorma@itq.upv.es](mailto:acorma@itq.upv.es); [mmoliner@itq.upv.es](mailto:mmoliner@itq.upv.es)

## Abstract

A Cu-SAPO-34 material with very high activity for selective catalytic reduction (SCR) of NO<sub>x</sub> and hydrothermal stability has been synthesized following a sequential rationalized design. By using specific combinations of organic structure directing agents (OSDAs) and gel compositions in a “one-pot” method, it was possible to control Cu occupancy, framework Si distribution, and to maximize the yield of solids. The amount of Cu<sup>2+</sup> is maximized and remains stable even after steaming at 750°C for 13 hours.

## Graphical abstract



## Highlights

- A rationalized methodology has allowed the one-pot synthesis of Cu-SAPO-34 zeotypes.
- An optimized Cu-SAPO-34 shows high activity and hydrothermal stability for SCR-NO<sub>x</sub>.
- Cu<sup>2+</sup> species remain in the optimized Cu-SAPO-34 even after severe ageing.

## Keywords

One-pot synthesis, silicoaluminophosphate, SAPO-34, selective catalytic reduction (SCR), nitrogen oxides (NO<sub>x</sub>)

## 1.- Introduction

The design of an attractive heterogeneous catalyst for a relevant chemical process, involves the synthesis of materials with high activity, selectivity, and stability. Moreover, if the catalyst is mean to be used industrially, the synthesis procedure should be economically competitive. In many cases, the combination of innovative work together with accumulated knowledge allows to achieve new synthesis that not only improves the physico-chemical properties of the catalysts but can meet the economical targets.

In the last years, the synthesis of small pore zeolites with large cavities containing extra-framework cationic metals, such as  $\text{Cu}^{2+}$ , has received much attention thanks to their excellent activity and stability for the selective catalytic reduction (SCR) of  $\text{NO}_x$ .<sup>[1]</sup> Traditionally, copper species are introduced in small pore zeolites by post-synthesis cationic exchange-impregnation methods.<sup>[1,2]</sup> However, the distribution of Cu within the zeolitic crystals following these procedures can be limited by diffusion of the Cu due to the presence of small pores (openings  $\sim 3.5 \text{ \AA}$ ), being the metal preferentially located close to the external surface.<sup>[3]</sup> To avoid this, different “one-pot” synthesis methods introducing organo-copper complexes in the synthesis gel have been recently described.<sup>[4]</sup> These direct procedures permit better metal dispersion within zeolitic crystals, and also allow reducing the overall synthesis steps required to achieve the final Cu-zeolite catalyst.<sup>[5]</sup> Diverse Cu-complexes and synthesis conditions have been reported in the last years to direct the “one-pot” preparation of different small pore chabazite (CHA) polymorphs, as Cu-SSZ-13,<sup>[4a,6]</sup> and Cu-SAPO-34.<sup>[4b,7]</sup> Despite the advances in the preparation, most of those materials present: low hydrothermal stability when treated under severe conditions (presence of steam at high temperatures),<sup>[4,7b]</sup> require the combination of expensive organic structure directing agents (OSDAs),<sup>[6]</sup> or their solid yields after crystallization are very low.<sup>[7a]</sup>

In a previous report, we have described the direct preparation of Cu-SAPO-34 using a combination of diethylamine (DEA) and Cu-tetraethylenepentamine (Cu-TEPA) as organic structure directing agents (OSDAs).<sup>[4b]</sup> In that study, we were able to synthesize Cu-SAPO-34 materials with high solid yields ( $>90\%$ wt of the initial oxide sources), and high catalytic activities for the SCR of  $\text{NO}_x$  under severe reaction

conditions when fresh and steamed samples at 600°C were tested. However, when the samples were more intensively steamed at 750°C for 13 hours, a significant loss of catalytic activity was observed for Cu-SAPO-34 materials containing low Cu content, while the crystalline framework of Cu-SAPO-34 materials with medium-high Cu content collapsed.<sup>[4<sup>b</sup>]</sup>

We present here an extensive and systematic study of the synthesis, characterization and catalytic testing of Cu-SAPO-34 that has allowed unveiling the key catalyst variables that control synthesis yield and hydrothermal stability. Then, by means of a one-pot synthesis procedure, it has been possible to prepare an efficient, very active and highly hydrothermally stable Cu-SAPO-34 catalyst. Deep characterization, including infrared spectroscopy (FTIR) using probe molecules, X-ray photoelectron spectroscopy (XPS) or temperature-programmed reduction (TPR) using H<sub>2</sub> as reducing gas, have shown the nature of the active sites and how they are preserved after hydrothermal treatment at 750°C.

## **2.- Experimental**

### **2.1.- Synthesis**

#### **2.1.1.- Direct syntheses of Cu-SAPO-34 materials**

In a general procedure for the Cu-SAPO-34 preparation, the Cu-complex was firstly prepared by mixing a 20%wt of an aqueous solution of copper (II) sulfate (98%wt, Alfa) with the tetraethylenepentamine (TEPA, 99%wt, Aldrich). This mixture was stirred for 2 hours until complete dissolution. Secondly, distilled water and phosphoric acid (85% wt, Aldrich) were added and stirred for 5 minutes. Third, alumina (75%wt, Condea) and silica (Ludox AS40 40%wt, Aldrich) sources were introduced in the gel mixture. Finally, diethylamine (DEA, 99%wt, Aldrich), tetraethylammonium bromide when required (TEABr, 99%wt Sigma-Aldrich), and SAPO-34 seeds (5%wt of expected final yield) were added into the gel, and the mixture was stirred for 30 minutes. The resulting gel was transferred to an autoclave with a Teflon liner, and heated at 150°C under static conditions for five days. Table 1 summarizes the experimental conditions used for the synthesis of each sample. Crystalline products were filtered and washed with abundant water, and dried at 100°C overnight. The samples were calcined at 550°C in air to properly remove the occluded organic species.

## 2.2.- Characterization

Powder X-ray diffraction (PXRD) measurements were performed with a multisample Philips X'Pert diffractometer equipped with a graphite monochromator, operating at 45 kV and 40 mA, and using Cu K $\alpha$  radiation ( $\lambda = 0,1542$  nm).

The chemical analyses were carried out in a Varian 715-ES ICP-Optical Emission spectrometer, after solid dissolution in HNO $_3$ /HCl/HF aqueous solution. The organic content of as-made materials was determined by elemental analysis performed with a SCHN FISIONS elemental analyzer.

MAS NMR spectra were recorded at room temperature with a Bruker AV 400 spectrometer.  $^{29}\text{Si}$  NMR spectra were recorded with a spinning rate of 5 kHz at 79.459 MHz with a 55 $^\circ$  pulse length of 3.5  $\mu\text{s}$  and repetition time of 180 s.  $^{13}\text{C}$  MAS NMR cross-polarization (CP) spectrum was recorded at a sample spinning rate of 5 kHz.  $^{29}\text{Si}$ , and  $^{13}\text{C}$  chemical shifts were referenced to tetramethylsilane, and adamantane, respectively.

UV-Vis spectra were obtained with a Perkin-Elmer (Lambda 19) spectrometer equipped with an integrating sphere with BaSO $_4$  as reference.

Temperature programmed reduction (TPR) experiments were performed in a Micromeritics Autochem 2910 equipment.

FTIR experiments were recorded with a Thermo "Nexus" spectrometer equipped with a DTGS detector. The infrared cell was designed to treat the samples in situ under vacuum or under flow conditions. For, CO and NO adsorption experiments, the sample has been activated under oxygen flow at 350 $^\circ\text{C}$  for 2h, followed by vacuum treatment ( $10^{-5}$  mbar) at 150 $^\circ\text{C}$  for 1h. Vacuum treatment under this condition is not reductive according to literature data.<sup>[8]</sup> After activation, the samples have been cooled down under vacuum conditions to -175 $^\circ\text{C}$ . At this temperature, CO or NO has been adsorbed in the pressure range between 0.2 and 2 mbar for CO and 0.05 and 0.6 mbar for NO. Decovolution of the IR spectra has been done using the ORIGIN software.

X-ray photoelectron spectra were collected using a SPECS spectrometer with a 150-MCD-9 detector and using a non monochromatic AlK $\alpha$  (1486.6eV) X-Ray source. Spectra were recorded at -175 $^\circ\text{C}$ , using analyzer pass energy of 30 eV, an X-ray power of 50W and under an operating pressure of  $10^{-9}$  mbar. During data processing of the

XPS spectra, binding energy (BE) values were referenced to P2p peak (135.5 eV). Spectra treatment has been performed using the CASA software.

### **2.3.- Catalytic experiments.**

The activity of the samples for the selective catalytic reduction (SCR) of NO<sub>x</sub> using NH<sub>3</sub> as reductor was tested in a fixed bed, quartz tubular reactor of 1.2 cm of diameter and 20 cm length. The total gas flow was fixed at 300 ml/min, containing 500 ppm of NO, 530 ppm of NH<sub>3</sub>, 7% of O<sub>2</sub>, and 5% of H<sub>2</sub>O. The catalyst (40 mg) was introduced in the reactor, heated up to 550 °C and maintained at this temperature for one hour under nitrogen flow. Then, the desired reaction temperature was set (170-550°C) and the reaction feed admitted. The NO<sub>x</sub> present in the outlet gases from the reactor were analyzed continuously by means of a chemiluminescence detector (Thermo 62C).

### **2.4.- Steaming procedures**

The hydrothermal treatment of metal-containing molecular sieves was performed by steaming the Cu-SAPO-34 samples with water (2.2 mL/min) at 750°C during 13 hours.

## **3.- Results**

### **3.1.- Previous direct syntheses of Cu-SAPO-34**

As referenced above, we were able to prepare different Cu-SAPO-34 materials in a one step synthesis procedure following a direct methodology that combines two different OSDAs, such as DEA and Cu-TEPA.<sup>[4<sup>b</sup>]</sup> Unfortunately, those Cu-SAPO-34 materials showed limited hydrothermal stability when aged under harder conditions (750°C for 13 hours).<sup>[4<sup>b</sup>]</sup> Indeed, the sample containing lower Cu content (see PXRD pattern of SAPO34-7\_HT750 in Figure 1B) showed better hydrothermal stability after steaming than the sample containing higher Cu-content (see PXRD pattern of SAPO34-8\_HT750 in Figure 1B), whose initial CHA structure was transformed into dense phase tridymite. Different Cu-containing zeolites have all shown lower hydrothermal stability when increasing their Cu-content.<sup>[1<sup>d</sup>,9]</sup> Nevertheless, besides Cu content, there are other

factors that can strongly influence the hydrothermal stability of SAPO-34. For instance, improving the ability of the zeolite to stabilize the extra-framework  $\text{Cu}^{2+}$  species by the appropriate distribution of negative charges within the zeolitic framework should favor the hydrothermal stability of the isolated cationic active sites and, consequently, the hydrothermal stability of the final catalyst. In the case of silicoaluminophosphates, framework negative charges are created by the adequate isomorphic substitution of  $\text{P}^{5+}$  with isolated  $\text{Si}^{4+}$  atoms in tetrahedral framework positions.<sup>[10]</sup> However, several times this chemical replacement occurs through multiple substitutions of Al and P with Si atoms, resulting in the formation of silicon-rich domains or silicon islands.<sup>[11]</sup> These Si-enriched areas do not create negative charges in the zeolitic crystal, and therefore, cationic species would not be efficiently distributed within the microporous material or they will be stabilized by very weak interactions with connectivity defects.

A further analysis of the catalytic activity for SCR of  $\text{NO}_x$  of the Cu-SAPO-34 samples synthesized in our previous study (SAPO34-7 and SAPO34-8)<sup>[4b]</sup> indicates that the most stable catalyst (SAPO34-7, which contains the lowest Cu-content) suffered a severe loss of activity after the steaming treatment (see SAPO34-7 and SAPO34-7\_HT750 in Figure 2). As introduced above, the overall hydrothermal stability after steaming of the SAPO34-7 is high from a crystallographic point of view (see the PXRD pattern of SAPO34-7\_HT750 in Figure 1B), but nevertheless the catalytic activity was strongly diminished after the harsh hydrothermal treatment.

SAPO34-7 sample was here studied by  $^{29}\text{Si}$  MAS NMR to evaluate the Si distribution into the final solid (see Figure 3). The results show that SAPO34-7 has more Si atoms forming Si-rich domains (signal at -110ppm) than isolated Si(4Al) environments (signal at -90 ppm). If this is so one can expect an inappropriate stabilization of cationic Cu species in the CHA cages by frameworks with Si-rich domains, and this could be a plausible explanation for the large catalytic activity loss after the steaming of the sample at 750°C. On the other hand, SAPO34-8 catalyst has also been studied by  $^{29}\text{Si}$  MAS NMR. Though SAPO34-8 shows a slight increase in the content of isolated Si atoms, the fact that Si-islands are still predominant, together with its much higher Cu-content (~6%wt Cu), results in a weaker crystalline structure when treated under severe hydrothermal conditions (see PXRD in Figure 1B).

At this point we can conclude that an improvement of the hydrothermal stability of Cu-SAPO-34 samples may require new synthesis conditions for the “one-pot” preparation that will drive into SAPO-34 samples with a better Si distribution, i.e. a larger amount of isolated Si-atoms through the zeolitic framework. Then, a good framework Si distribution combined with a low-medium metal content (less than 6%wt Cu), may direct towards more hydrothermally stable Cu-SAPO-34 samples. In other words, a one-pot synthesis procedure should be developed to control the total amount and dispersion of Si in framework positions.

### **3.2.- Direct synthesis of Cu-SAPO-34 with controlled Si distributions**

#### **3.2.1.- Synthesis and characterization**

We started the direct synthesis of new Cu-SAPO-34 materials with less Si (Si/Al ratios of 0.19 instead of 0.36) and less Cu-complex [Cu-TEPA/(Al+P) ratios of 0.025-0.05 instead of 0.05-0.10] in the synthesis gels (see entries Cu-1 and Cu-2 in Table 1). To favor the nucleation and crystallization of CHA materials, a small amount of SAPO-34 crystals (5%wt) was also introduced in the synthesis gels (see Table 1). The PXRD patterns of Cu-1 and Cu-2 solids reveal highly crystalline SAPO-34 materials (see Figure 1A).

However, very different solid yields have been obtained for both materials: (~90%wt and ~40%wt of initial oxide sources for Cu-1 and Cu-2 respectively, see Table 2). This result was surprising since the unique difference in the two syntheses was the amount of Cu-complex in the gels (0.05 and 0.025 for Cu-1 and Cu-2, respectively, see Table 1). The low solid yield observed for the Cu-2 catalyst would indicate that most of the heteroatoms introduced in the initial gel remained in solution after the crystallization process. Chemical analyses on those samples reveal that Cu-1 and Cu-2 samples show close Cu/TO<sub>2</sub> ratios of 0.062 and 0.051, respectively (see Table 2).

Moreover, both samples present a similar content of Cu-TEPA and DEA in the as-prepared catalysts (see elemental analyses in Table 3). The UV-Vis spectra of the two as-prepared samples show a single band centered at 260 nm, which has been assigned to the presence of intact Cu-TEPA molecules (see Figure 4). Interestingly, if the metal content for those two samples is calculated in terms of metal atoms per cavity (note that the unit cell of CHA has 36 T-atoms, and each unit cell has two CHA cavities, see

Figure 5-a), it appears that in both cases almost one Cu specie per CHA cavity should occur (see Table 2). This is an important result, since it allows concluding that Cu-TEPA, even when present at low concentrations in the synthesis gels, has a higher directing effect towards CHA cages than diethylamine. In fact, it is possible to fill every CHA cage with one Cu-TEPA molecule. The results then would suggest that, under the two tested synthesis conditions, the crystallization of SAPO-34 material is limited by the Cu-TEPA content in the gel. Therefore, it seems that Cu-TEPA complex molecules not only show a high structure directing effect towards CHA cavities (one Cu-TEPA/cavity), but also they are able to determine the crystal growth and, consequently, the overall solid yield depending on their initial content.

Observing the unique directing effects of Cu-TEPA, the role of DEA in the cooperative direct synthesis of Cu-SAPO-34 should be discussed. To find if DEA molecules play a significant role as co-OSDA for the efficient direct synthesis of Cu-SAPO-34 materials, blank experiments without DEA, under similar synthesis conditions to Cu-1 and Cu-2, were carried out. The solids obtained in absence of DEA were trydimite, confirming the importance of DEA molecules for the one-pot crystallization of Cu-SAPO-34.

Concerning the silicon distribution within Cu-1 and Cu-2 catalysts as compared to previously reported SAPO34-7 and SAPO34-8, the results in Figure 3 indicate that Cu-1 and Cu-2 materials present an improved Si distribution in the crystalline solids. Indeed, a considerably decrease of Si-rich domains (signal at -110 ppm) is observed within the samples. These results are in agreement with our hypothesis on the positive effect of reducing the Si content in the synthesis mixture. It is noticeable the ideal Si distribution achieved for Cu-2 catalyst, for which only well-distributed and isolated Si atoms (signal at -90 ppm) are observed. Therefore, different initial Cu-TEPA contents in the synthesis gels have an effect not only on the catalyst solid yield, but also on the Si distribution.

### **3.2.2.- Catalytic activity and hydrothermal stability**

Taking into account all the above, it becomes clear that a correlation between synthesis conditions (i.e. gel composition), framework composition, catalytic activity, and zeolite stability, must exist. Then, firstly, the catalytic activity of calcined Cu-1 and Cu-2 materials has been evaluated for the SCR of NO<sub>x</sub>. As seen in Figure 2-A, Cu-1 and Cu-2 catalysts show very high NO<sub>x</sub> conversion with values above 95% under a broad range of reaction temperatures (250-450°C). Their catalytic behavior is very similar to

the one observed for our previous optimum catalyst SAPO34-8, which presented similar Cu content, though SAPO34-8 shows low hydrothermal stability when steamed at 750°C for 13 hours. This low stability was explained by the high content of Cu atoms combined with the presence of a large amount of Si-islands, which would prevent efficient Cu stabilization. The hydrothermal stability of Cu-1 and Cu-2 catalysts has also been evaluated in presence of steam at 750°C for 13 hours. As seen in Figure 1-B, the PXRD pattern of Cu-1 material (Cu-1\_HT750) reveals the complete loss of CHA structure after the steaming process, while the PXRD pattern of Cu-2 (Cu-2\_HT750) mostly preserves the original CHA structure with a very small amount of tridymite dense phase formation (see small peak at 21.5 degrees). The low hydrothermal stability of Cu-1 can be attributed to its high Cu content (6.6%wt, see Table 2) and the presence of Si islands, while the Cu-2 sample performs much better when severely steamed due to the presence of some lower Cu-content (5.4%wt, see Table 2) combined with an excellent Si dispersion within CHA framework (see Cu-2 in Figure 3). The catalytic activity of Cu-2 catalyst after being severely aged has been studied for the SCR of NO<sub>x</sub>. As seen in Figure 2-B, this steamed material mostly retains its original catalytic activity, showing NO<sub>x</sub> conversion values close to 90% under a broad temperature range (250-450°C). Very interestingly, the aged Cu-2 catalyst (Cu-2\_HT750) shows a much higher catalytic activity than our previous hydrothermally stable SAPO-34 catalyst at 750°C (see SAPO34-7\_HT750 in Figure 2-B).<sup>[4b]</sup> At this point, we can conclude that it is possible to design a Cu-containing SAPO-34 material with excellent catalytic properties and hydrothermal stability by using a simple and inexpensive direct synthesis methodology. However, from an industrial point of view, the synthesized catalyst not only must show excellent physico-chemical properties, but also its synthesis procedure must be cost efficient. From this point of view, though synthesis raw materials used for the SAPO-34 preparation are reasonable low-cost, the zeolite yield should be clearly improved.

### **3.3.- Direct synthesis of Cu-SAPO-34 materials with high solid yield and controlled Cu-content**

#### **3.3.1.- Preliminary screening**

The attractive results achieved in the previous section when low Cu-TEPA contents were introduced in the reaction mixture, directed us to systematically study other different synthesis conditions using low Cu-TEPA/(Al+P). The objective was to direct the crystallization of hydrothermally stable SAPO-34 materials with higher yields. Six new syntheses with three different P/Al ratios (0.8, 0.75, 0.7) and two different Cu-TEPA/(Al+P) ratios (0.025, 0.05) were performed (see synthesis conditions in Table 1). As it can be seen in Figure 6-A, the PXRD patterns of all as-prepared materials show the CHA structure after 5 days at 150°C. However, the three Cu-SAPO-34 materials synthesized using the lowest Cu-TEPA/(Al+P) ratio (0.025), show very low solid yields (<46%wt of the initial oxides, see Cu-4, Cu-6, and Cu-8 in Table 2). These results are in agreement with the solid yield achieved for Cu-2 material, that was also prepared with 0.025 Cu-TEPA/(Al+P) ratio in the reaction mixture. Therefore, the results confirm that the crystallization of SAPO-34 under our synthesis conditions is limited by the Cu-TEPA content in the gel, and this variable is determinant for the overall solid yield achieved. Since our first aim is to find an efficient preparation for the Cu-SAPO-34 material with high solid yields, these materials were not considered further.

The other three crystalline Cu-SAPO-34 materials synthesized using a Cu-TEPA/(Al+P) ratio of 0.05, give solid yields higher than 85%wt (see Cu-3, Cu-5, and Cu-7 in Table 2). Similar solid yield was achieved for Cu-1 zeolite, which was also synthesized using a theoretical Cu-TEPA/(Al+P) ratio of 0.05.

When the catalytic activity for SCR of NO<sub>x</sub> of samples Cu-3, Cu-5, and Cu-7 was studied, results in Figure 7 show very high activity, with NO<sub>x</sub> conversions close to 100% in a broad reaction temperature range (200-500°C). Interestingly, these samples exhibit different stability behavior after being steamed at 750°C for 13 h. Cu-3 material presents the lowest hydrothermal stability after being aged at 750°C, observing a large transformation of CHA structure into trydimite dense phase (see PXRD pattern of Cu-3\_HT750 in Figure 6-B). On the other hand, Cu-5 and Cu-7 are more stable, but some transformation into trydimite dense phase is also detected (see PXRD patterns of Cu-5\_HT750 and Cu-7\_HT750 in Figure 6-B).

ICP analyses of these three materials reveal comparable Cu-contents (~6%wt, see Table 2), that would result in one Cu atoms per CHA cavity. The partial hydrothermal stability improvement of Cu-5 and Cu-7 materials would occur by the larger presence

of silicon atoms in the SAPO-34 frameworks (Si/TO<sub>2</sub> values are 0.104, 0.112 and 0.122 for Cu-3, Cu-5 and Cu-7, respectively).

Thus, Cu-SAPO-34 materials with good solid yields and catalytic activities are achieved, but some hydrothermal stability improvement is still required.

### **3.3.2.- Cu-SAPO-34 synthesis by triple-OSDA combination**

As observed previously for the SSZ-39 zeolite, which is a zeolite presenting also D6R in its structure, the hydrothermal stability of this small pore zeolite can be clearly improved by reducing the overall Cu content.<sup>[1<sup>d</sup>]</sup> However, we have reported in the present work a considerably decrease of the solid yield when the Cu-TEPA content in the reaction mixture is decreased and, at the same time, the crystallized Cu-SAPO-34 materials always contain almost one Cu atom per CHA cavity (see Cu-2 and Cu-4 in Table 2). It seems that when very low amount of Cu-TEPA molecules are introduced in the preparative gel, our “one-pot” synthesis methodology is not able to direct the formation of crystalline Cu-SAPO-34 with significant lower Cu content (much less than one Cu atom per CHA cavity).

We have found that small diethylamine (DEA) molecules are also incorporated in the final solids (see elemental analyses of Cu-1 and Cu-2 in Table 3, and solid <sup>13</sup>C MAS NMR of Cu-2 in Figure 8), but they act as simply pore fillers. Therefore, a real competition of DEA with cationic Cu-TEPA complexes for templating CHA cavities cannot be claimed, and because of that, Cu content was always constant in the final solids. Therefore, if we want to decrease the incorporation of Cu-TEPA, a molecule with a stronger structure directing effect than DEA should be introduced. This will compete with Cu-TEPA and by mastering the concentration of the new OSDA and Cu-TEPA in the synthesis gel, it could be possible to control the level of Cu present in the one-pot synthesis of Cu-SAPO-34. For doing that we have selected the tetraethylammonium (TEA) cation, which has been thoroughly described as an efficient OSDA for the synthesis of SAPO-34.<sup>[11]</sup> We were expecting that the TEA molecules will compete with the cationic Cu-TEPA complex during the nucleation and crystallization of SAPO-34 allowing to reduce the total amount of copper atoms per unit cell while still achieve large solid yields.

Since the synthesis conditions used for the preparation of the Cu-7 material gave excellent solid yields and acceptable hydrothermal stability, those synthesis conditions were selected and a gel with TEA, DEA, and Cu-TEPA as triple-cooperative OSDAs was prepared and crystallized (see Cu-9 in Table 1).

The PXRD pattern of the as-prepared Cu-9 material reveals a fully-crystalline SAPO-34 structure (see Figure 9), with a final solid yield higher than 90%wt of the initial oxide sources (see Table 2). UV-Vis spectrum of the as-prepared Cu-9 sample indicates that Cu-TEPA complex molecules remain intact after the crystallization process within zeolitic crystals (see Cu-9 in Figure 4). In addition, ICP analysis on Cu-9 material shows that the Cu content has been clearly reduced to 3.3%wt Cu (see Table 2), which correspond to 0.6 Cu atoms per CHA cavity. In order to verify that the Cu-content decrease has occurred by the partial replacement of Cu-TEPA by TEA molecules, the as-prepared Cu-9 sample has been characterized by elemental analysis and solid  $^{13}\text{C}$  MAS NMR spectroscopy. The as-prepared Cu-9 shows a C/N ratio of 3.4, which is higher than the values observed for as-prepared TEA-free Cu-1 and Cu-2 samples (C/N  $\sim$  2.1-2.2, see Table 3). This analysis is not conclusive to claim that TEA molecules are partially replacing Cu-TEPA complex molecules in the as-prepared Cu-9 sample, since a possible increase of the DEA content would result also in an increase of the C/N ratio (note that TEPA, DEA, and TEA molecules show a C/N ratio of 1.6, 4, and 8, respectively). Nevertheless, the solid  $^{13}\text{C}$  MAS NMR spectrum undoubtedly show the characteristic two bands of TEA molecules at 6.3 and 52.1 ppm (see Cu-9 in Figure 8), confirming the partial replacement of Cu-TEPA by TEA molecules.

The Si distribution in the calcined Cu-9 material has also been studied by solid  $^{29}\text{Si}$  MAS NMR spectroscopy. As seen in Figure 10, a mixture of isolated Si species (signal centered at -90 ppm), and Si-rich domains (signal centered at -110 ppm) can be observed in Cu-9 material. From what was said before, it appears that an ideal Si distribution has not been accomplished in Cu-9 as occurred with Cu-2 sample. Nevertheless, Cu-9 material shows much higher solid yield and controlled Cu-content (0.6 Cu atoms per CHA cavity), and deserves to be further studied to determine its catalytic activity and hydrothermal stability.

### **3.3.3.- Catalytic activity and hydrothermal stability**

The calcined Cu-9 sample has been tested for the SCR of NO<sub>x</sub>, and as it can be seen in Figure 11, this material shows very high catalytic activity with NO conversion values above 90% under a wide reaction temperature range (200-450°C). Very interestingly, the PXRD pattern of the Cu-9 after being steam-treated at 750°C for 13 hours presents a negligible presence of the tridymite dense phase (almost inexistent peak at 21.5 degrees, see Cu-9\_HT750 in Figure 9), revealing its high hydrothermal stability. Indeed, as we hypothesized above, the ability of preparing a Cu-SAPO-34 material with lower Cu-content by direct methods results in a more stable catalyst.

The catalytic activity of the steamed Cu-9 material is analogous to the fresh Cu-9 material (see Figure 11), probably indicating that the local copper environments have not significantly changed after the hydrothermal treatments.

#### **3.3.4.- Catalytic active sites characterization**

In order to determine the type of copper species before and after ageing procedures, fresh and steamed Cu-9 materials have been properly characterized by temperature-programmed reduction (TPR) using hydrogen, FTIR spectroscopy of adsorbed probe molecules, as CO and NO and XPS.

The H<sub>2</sub>-TPR results of fresh and steamed Cu-9 samples show very similar profiles (see Figure 12). The H<sub>2</sub> consumption peaks observed from 200 to 500°C indicate the presence of three different types of copper species coexisting in the catalysts. According to literature,<sup>[12]</sup> the peaks located at lower temperatures (~250-270°C) represent the reduction of isolated Cu<sup>2+</sup>,<sup>[13]</sup> the peaks centered at 350-370 represent the reduction of bulk CuO to Cu<sup>0</sup>,<sup>[14]</sup> and finally, the higher temperature peaks can be assigned to the reduction of Cu<sup>+</sup> to Cu<sup>0</sup>.<sup>[13]</sup> As seen in Figure 12, the higher intensity of the H<sub>2</sub> consumption peak at 250°C indicates that Cu<sup>2+</sup> is the predominant cupric specie in both, fresh and steamed, Cu-9 samples. The asymmetry to lower reduction temperatures observed in the fresh sample point to some heterogeneity of Cu<sup>2+</sup> ion species. On the other hand, the small peaks observed in both materials at 350°C and 450°C, could be attributed to small amounts of CuO and Cu<sup>+</sup> species, respectively. XPS data shows, in agreement to the TPR data, the existence of highly dispersed Cu<sup>2+</sup> ions (BE 936.8eV), being this the predominant specie, in addition to CuO (BE 933.4eV), in both fresh and steamed Cu-9 samples (see Figure 13).<sup>[15]</sup>

To analyze in more detail the nature of Cu species, fresh and aged Cu-9 samples have been studied by FTIR spectroscopy using CO and NO as probe molecules. Both molecules are very sensitive to the local environment of Cu ions, being able to discriminate between different oxidation and coordination states. Thus CO is a very selective molecule for the determination of Cu<sup>+</sup> species but does not allow the determination of Cu<sup>2+</sup> cations.<sup>[16]</sup> In contrast, NO interacts efficiently with both Cu<sup>2+</sup> and Cu<sup>+</sup>, being more selective towards Cu<sup>2+</sup> species.<sup>[17]</sup>

As seen in Figure 14, two main bands centered at 2175 and 2148 cm<sup>-1</sup> appeared for both Cu-9 samples in the FTIR spectra of CO adsorption. These bands are associated with the symmetric and asymmetric stretching modes of the [Cu<sup>+</sup>(CO)<sub>2</sub>] complex.<sup>[16c,18]</sup> Therefore, Cu<sup>+</sup> ions are present in both fresh and steamed samples, but their relative amount compared to Cu<sup>2+</sup> ions cannot be determined by FTIR spectroscopy using CO as probe molecule.

Regarding the nature of Cu<sup>2+</sup> ions, the IR spectra of NO adsorption shows some heterogeneity evidenced by the coexistence of several bands in the 1950-1880 cm<sup>-1</sup> IR region of the  $\nu_{\text{NO}}$  vibration on both fresh and aged Cu-9 samples (see Figure 15). NO molecules interacting with isolated Cu<sup>2+</sup> ions in square pyramidal configuration has been evidenced at 1912 and 1905cm<sup>-1</sup>, while bands at higher frequencies has been assigned to associated Cu<sup>2+</sup> sites.<sup>[16a,17]</sup> On the other hand, NO interacting with the OH group of [Cu-OH]<sup>+</sup> species is expected at lower frequencies (1898-1880cm<sup>-1</sup>).<sup>[16a,19]</sup> In the lower frequency region (1806-1780 cm<sup>-1</sup>), the IR band at 1755 cm<sup>-1</sup> is associated to Cu<sup>+</sup> mononitrosyl complex [Cu<sup>+</sup>(NO)].<sup>[20]</sup> According to the results obtained from FTIR characterization, Cu species in different coordination environment and oxidation state can be found in fresh and steamed Cu-9 catalysts. However, FTIR spectra of NO adsorption, XPS and H<sub>2</sub>-TPR clearly indicate that dispersed Cu<sup>2+</sup> ions, either as isolated or low associated Cu<sup>2+</sup> ions, are the predominate species in both Cu-9 samples. Interestingly, these Cu<sup>2+</sup> species are very stable to harsh hydrothermal treatments, as indicated by the H<sub>2</sub>-TPR profile and FTIR spectra for Cu-9 after being severely steamed at 750°C for 13 hours.

Finally, the FTIR spectra of NO adsorption on Cu-9 and SAPO34-7 samples, both fresh and aged at 750°C, have been compared. As it can be seen in Figure 16a, these catalysts show different intensities for the bands associated to Cu<sup>2+</sup> species (1950-1880

cm<sup>-1</sup>). Among these species, while the nature of the active catalytic sites for the SCR of NO<sub>x</sub> remains open to discussion, our data, interestingly shows a linear correlation between the IR area associated to the 1910 and 1898 cm<sup>-1</sup> IR bands in the NO-FTIR spectra and the catalytic activity for the SCR of NO<sub>x</sub> for each catalyst (see Figure 16b). These results agree with the assessment of isolated Cu<sup>2+</sup> ions in square pyramidal configuration or [Cu-OH]<sup>+</sup> species as potential active sites.

#### **4.- Conclusions**

A sequential, rationalized synthesis design has allowed the “one-pot” direct preparation of Cu-SAPO-34 materials with very high solid yields, improved physico-chemical properties, and high hydrothermal stability. It has been shown that the control of Cu-TEPA and Si contents in the synthesis gels combined with specific combinations of multiple OSDAs (Cu-TEPA, DEA, and TEA) allows tailoring the physico-chemical properties of the resultant Cu-SAPO-34 catalysts. An optimized Cu-SAPO-34 material presents excellent catalytic properties for the SCR of NO<sub>x</sub> and very high hydrothermal stability when steamed under severe conditions (750°C for 13 hours). Cu-SAPO-34 catalysts were properly characterized by FTIR spectroscopy using probe molecules (CO and NO), XPS and temperature programmed reduction (TPR) using H<sub>2</sub> in order to illustrate the catalytic active sites. A large proportion of Cu in the optimized Cu-SAPO-34 is in the form of Cu<sup>2+</sup> species even after steam treatment.

#### **Acknowledgements**

This work has been supported by Haldor-Topsoe, the Spanish Government through Consolider Ingenio 2010-Multicat, the “Severo Ochoa Program”, MAT2012-37160; and by UPV through PAID-06-11 (n.1952). Manuel Moliner also acknowledges to “Subprograma Ramon y Cajal” for the contract RYC-2011-08972. The authors thank Isabel Millet for technical support.

Figure 1: PXRD patterns of as-prepared Cu-SAPO-34 materials synthesized following the synthesis conditions reported in Table 1 (A), and after being steam-treated at 750°C for 13 hours (B)

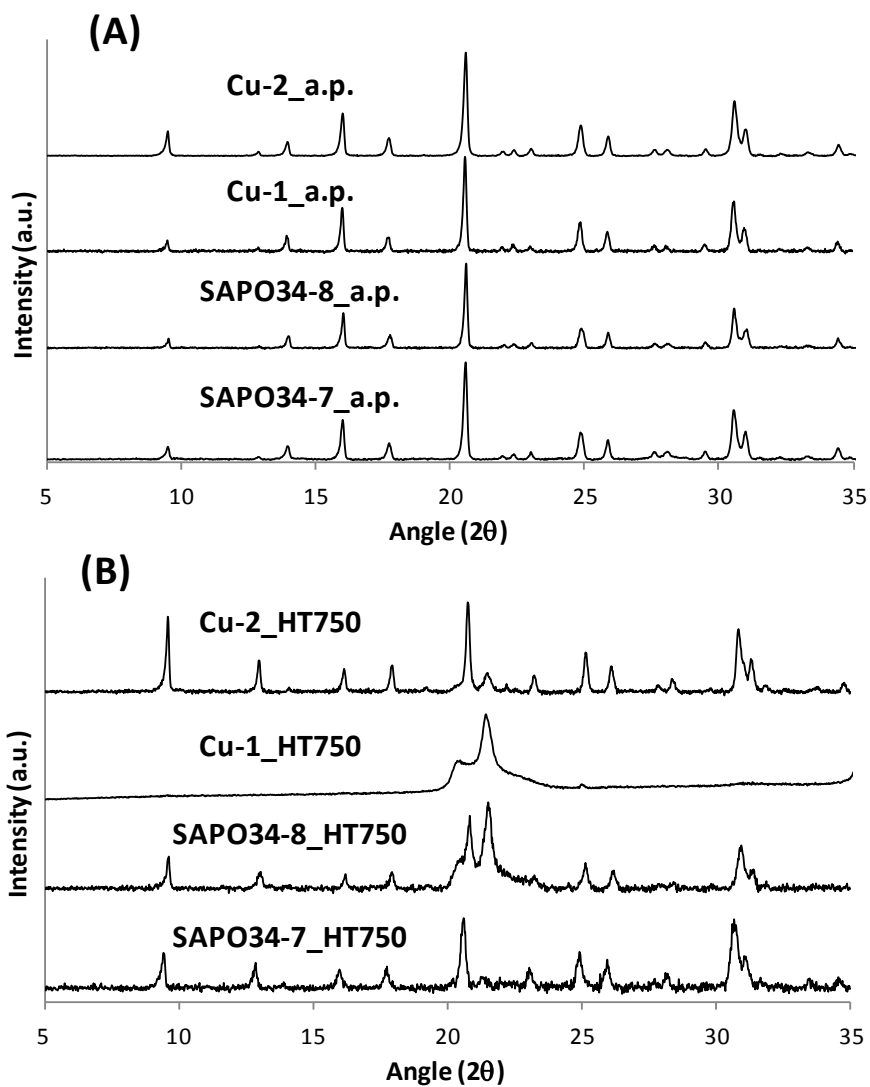


**Figure 2: Catalytic activity for the SCR of NO<sub>x</sub> reaction of fresh Cu-SAPO-34 materials synthesized according Table 1 (A) and after being steam-treated at 750°C for 13 hours (B)**

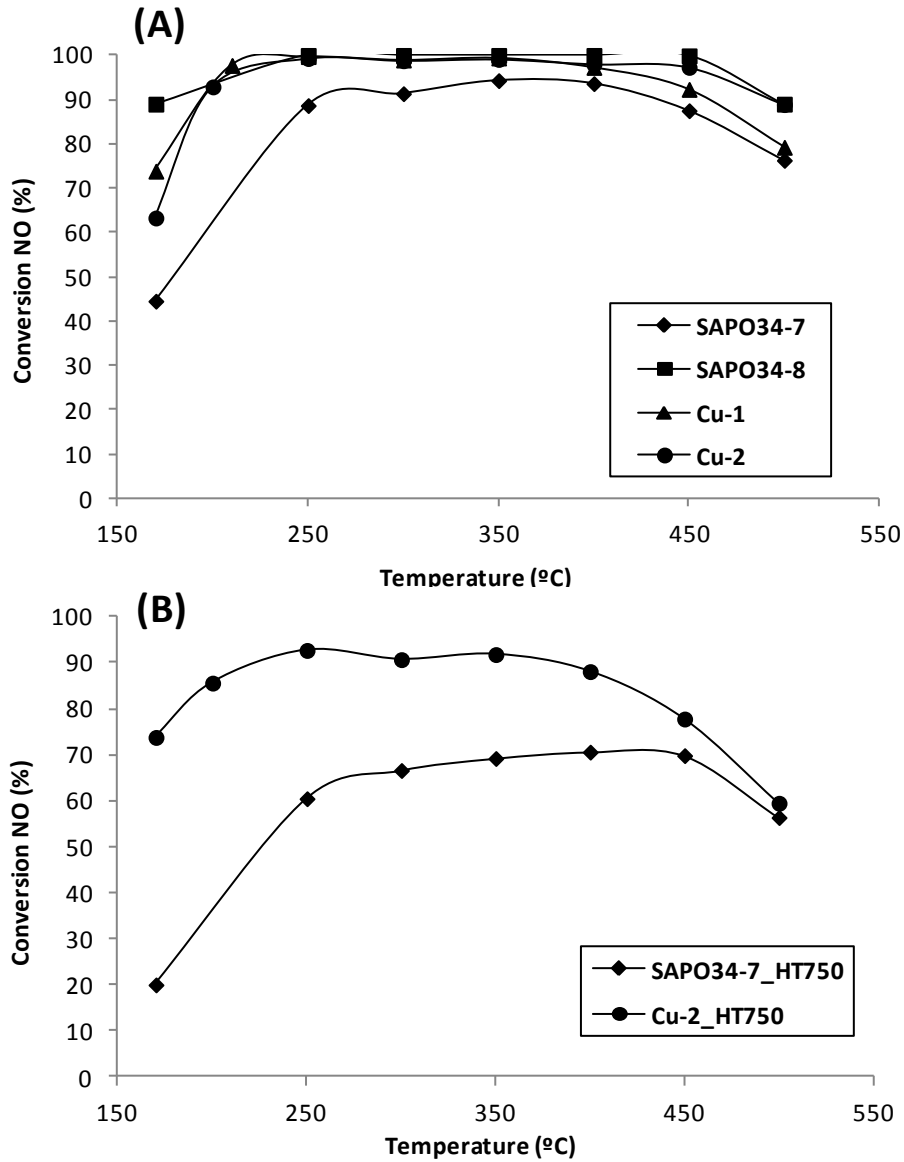
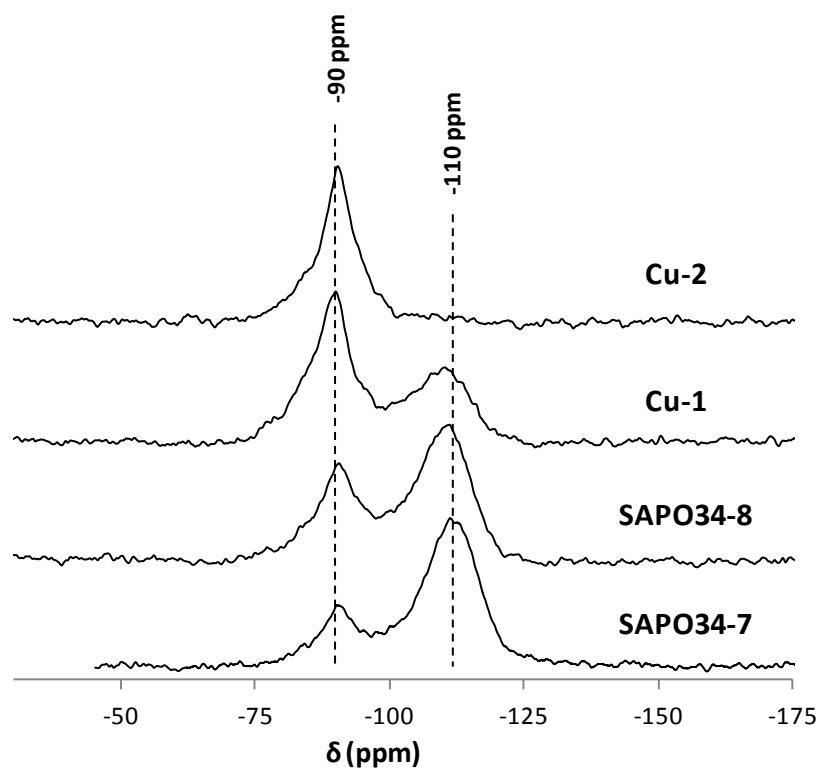
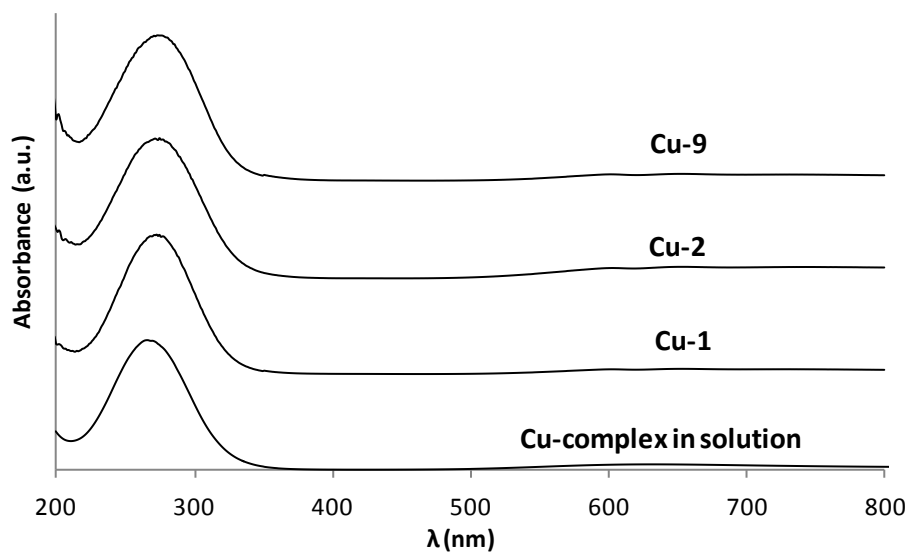


Figure 3: Solid  $^{29}\text{Si}$  MAS NMR spectra of Cu-SAPO-34 materials synthesized according

Table 1



**Figure 4: UV–Vis spectra of Cu-TEPA complex in solution, and as-prepared Cu-SAPO-34 materials synthesized according Table 1**



**Figure 5: Unit cell of CHA zeolite**

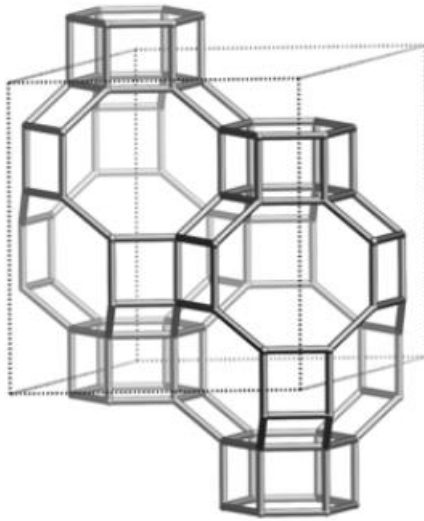


Figure 6: PXRD patterns of as-prepared Cu-SAPO-34 materials synthesized following the synthesis conditions reported in Figure 1 (A), and after being steam-treated at 750°C for 13 hours (B)

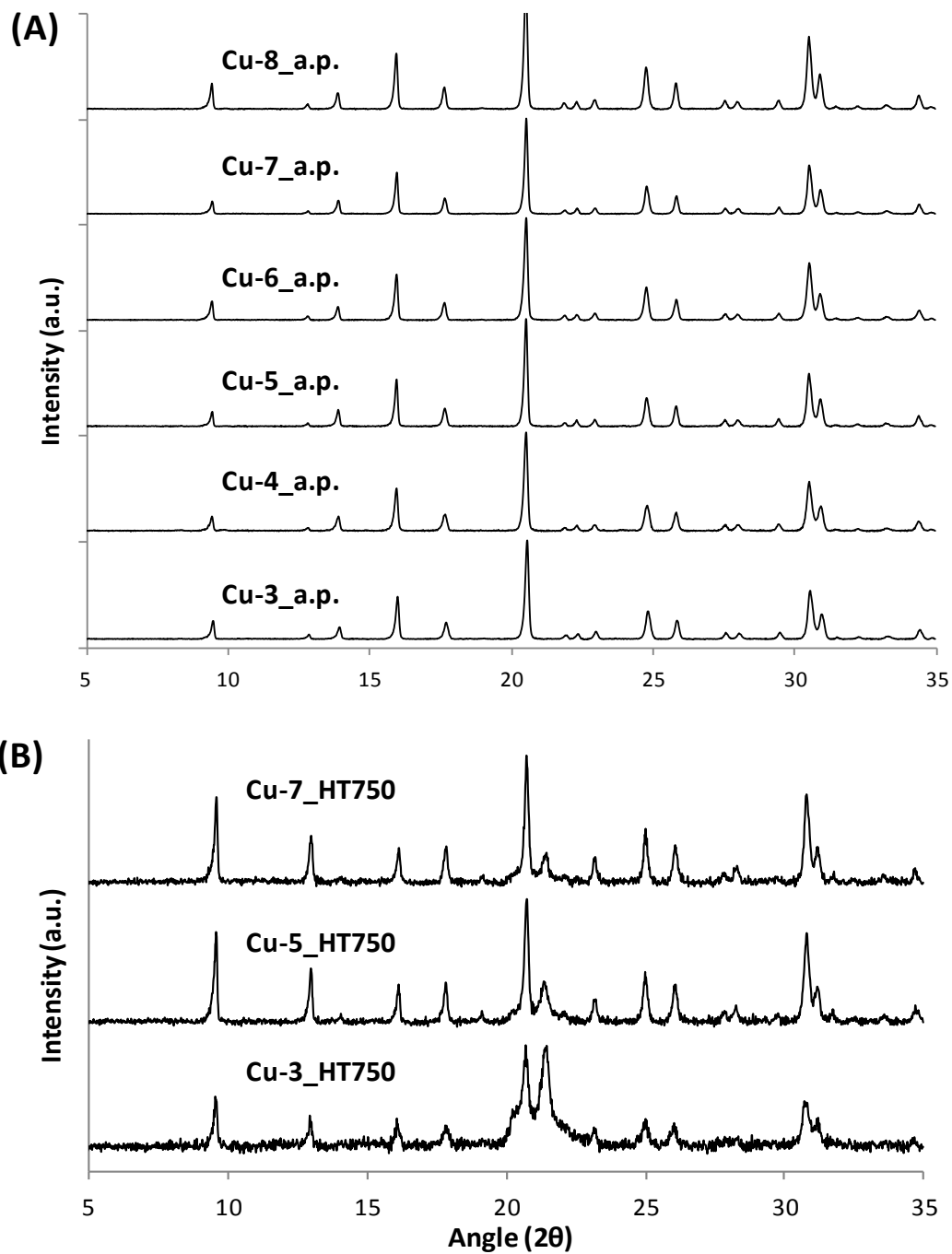


Figure 7: Catalytic activity for the SCR of NO<sub>x</sub> reaction of fresh Cu-3, Cu-5, and Cu-7 materials synthesized according Table 1

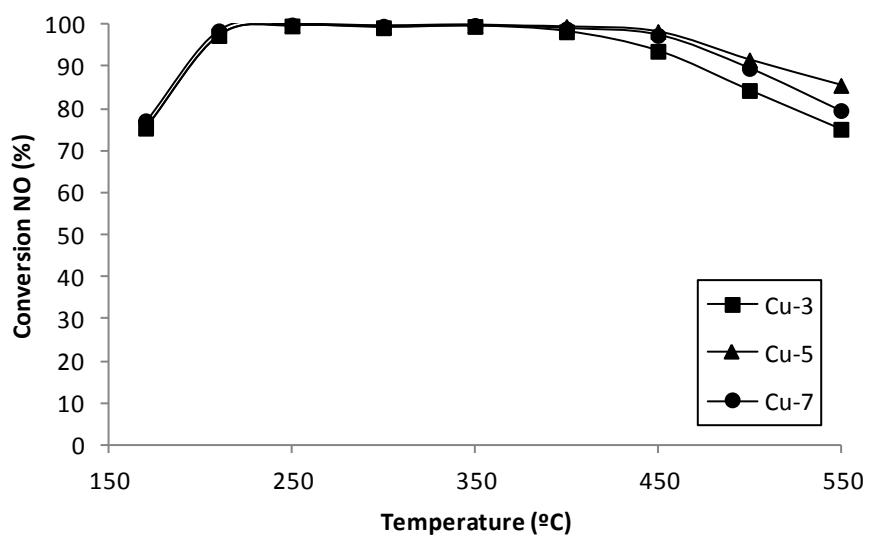


Figure 8: Solid  $^{13}\text{C}$  MAS NMR of as-prepared Cu-2 and Cu-9 samples, and liquid  $^{13}\text{C}$  MAS NMR of DEA, TEA and TEPA

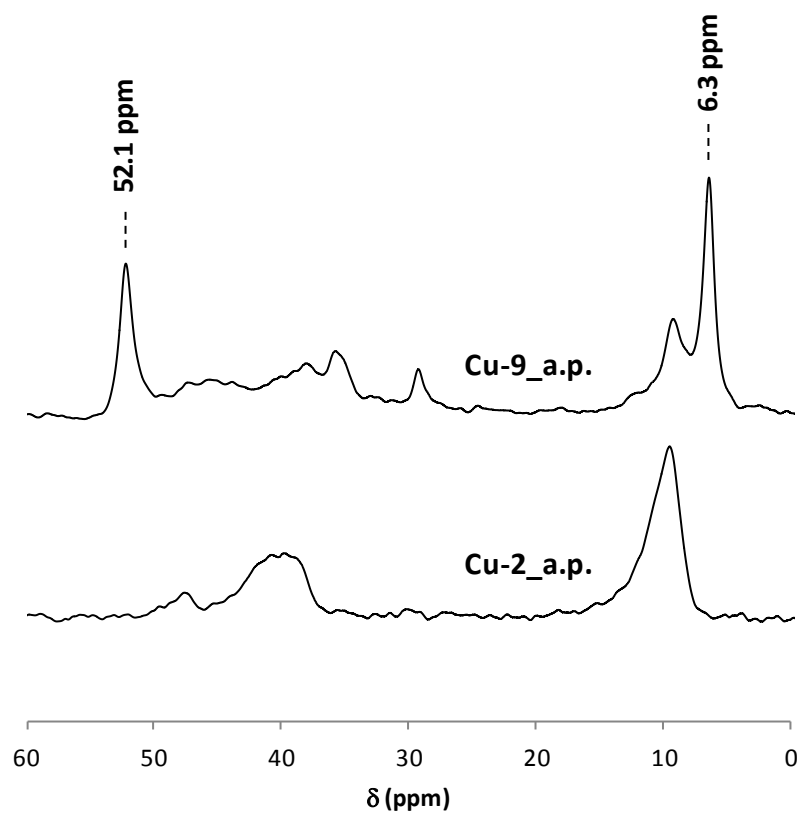


Figure 9: PXRD patterns of the as-prepared Cu-9 sample (Cu-9\_a.p.) and after being hydrothermally treated at 750°C for 13 hours (Cu-9\_HT750)

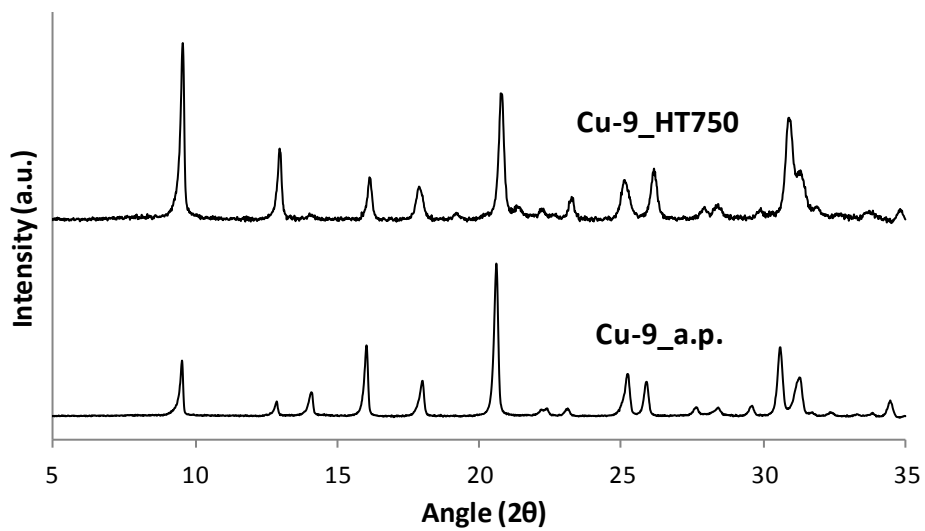
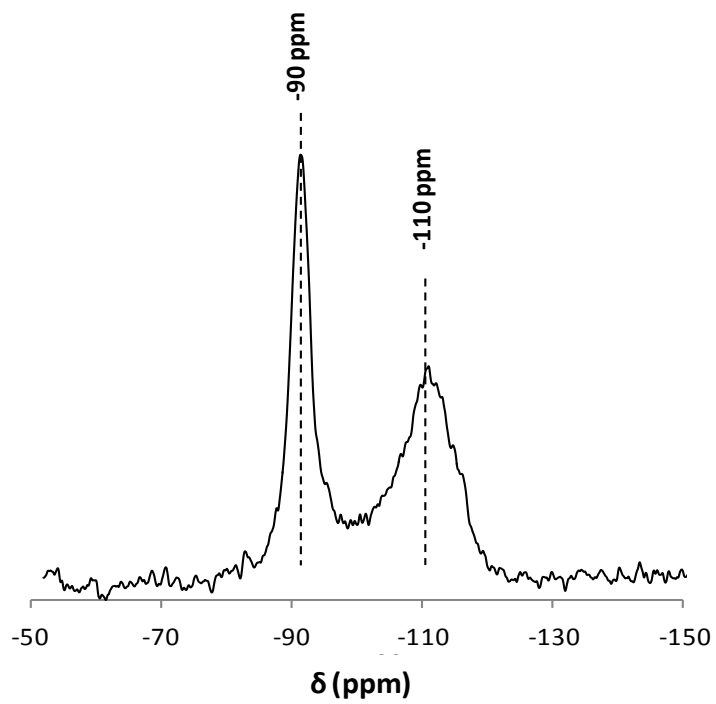


Figure 10: Solid  $^{29}\text{Si}$  MAS NMR of calcined Cu-9 sample



**Figure 11: Catalytic activity for the SCR of NO<sub>x</sub> reaction of fresh Cu-9 material, and after hydrothermal treatment at 750°C for 13 hours**

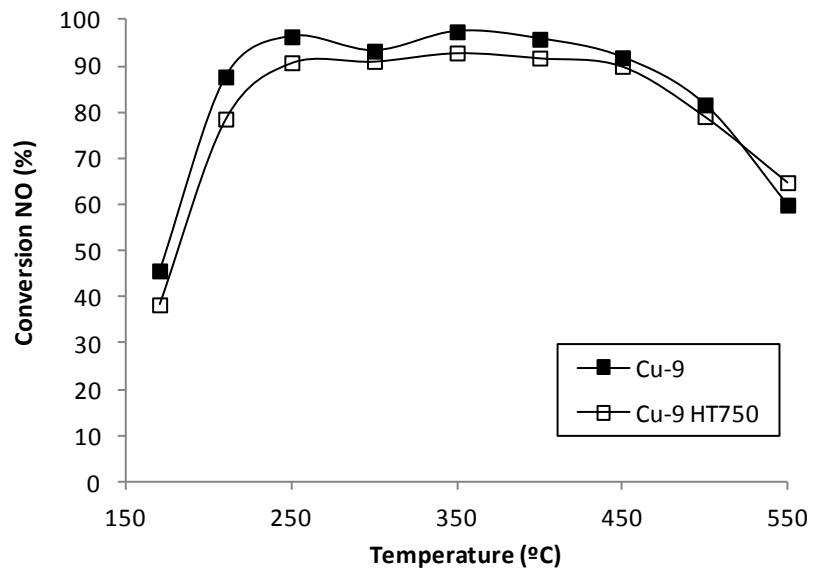


Figure 12: H<sub>2</sub>-TPR profile of calcined Cu-9 (A) and after being aged at 750°C for 13 hours (B)

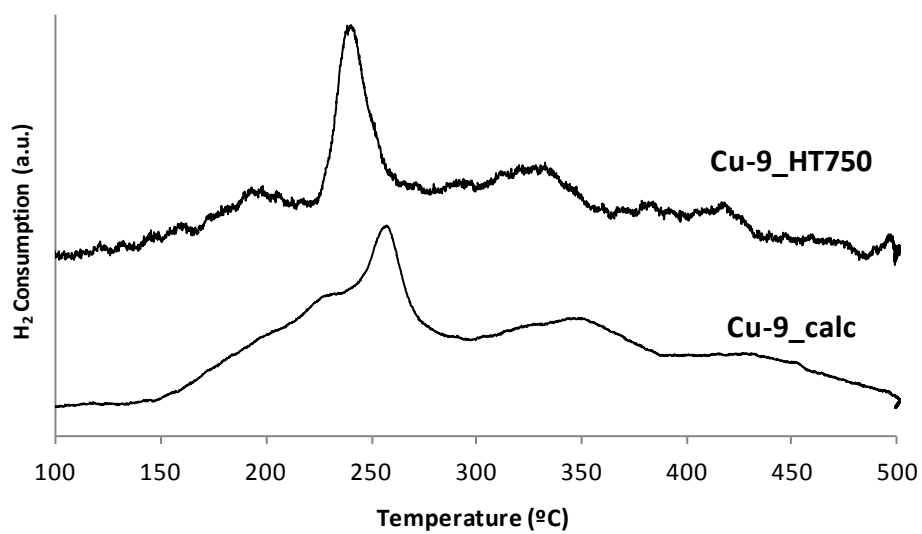
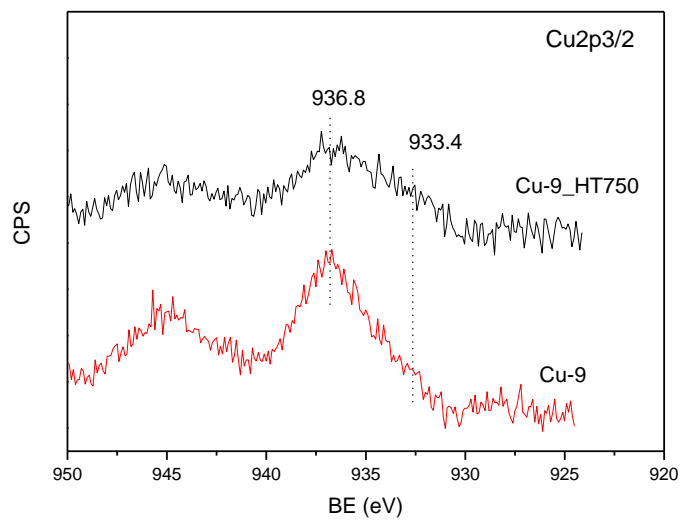


Figure 13: Cu $2p_{3/2}$  XPS line of the Cu-9 and Cu-9\_HT750 samples



**Figure 14: FTIR spectra of CO adsorbed at -175°C on calcined Cu-9 (A) and after being aged at 750°C during 13 hours (B). Each sample has been measured at increasing CO pressures: 0.45-0.50 (a), 0.65-0.71 (b), 0.85-0.90 (c), 1.0-1.10 (d), 1.25-1.35 (e) and 1.45-1.52 mbar (f)**

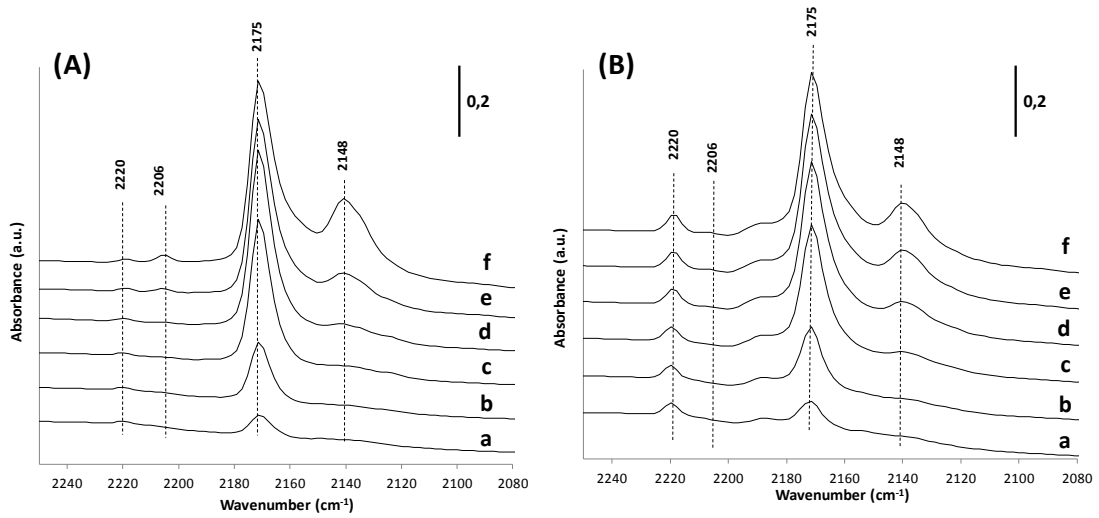
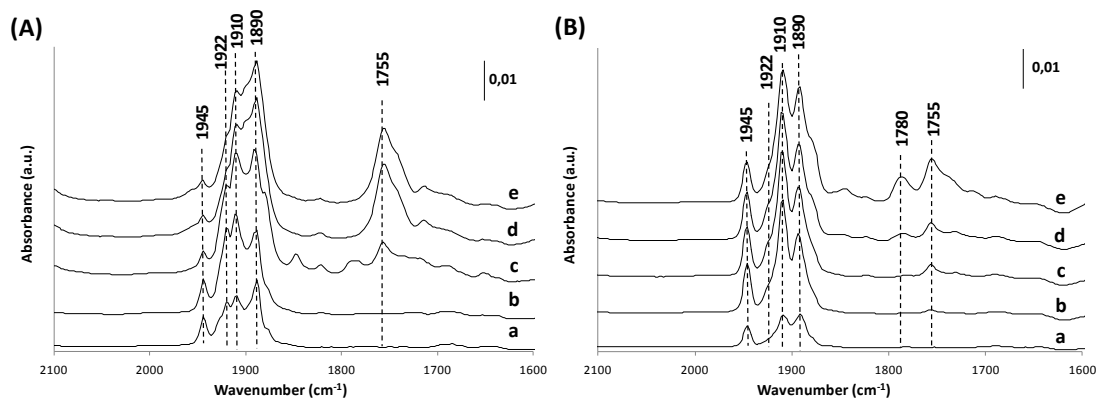
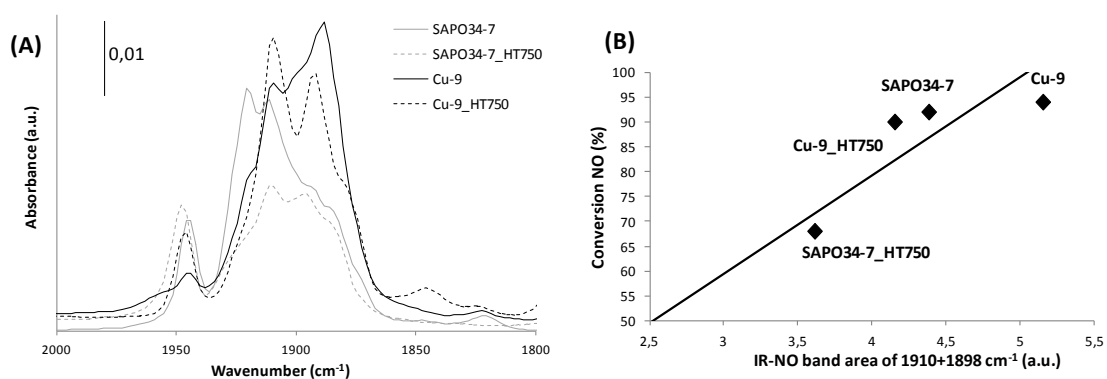


Figure 15: FTIR spectra of NO adsorbed at  $-175^{\circ}\text{C}$  on calcined Cu-9 (A) and after being aged at  $750^{\circ}\text{C}$  during 13 hours (B). Each sample has been measured at increasing NO pressures: 0.10-0.12 (a), 0.20-0.23 (b), 0.28-0.31 (c), 0.45-0.51 (d), and 0.57-0.62 mbar

(e)



**Figure 16: (A) FTIR spectra of NO adsorbed at -175°C on fresh and steamed at 750°C SAPO34-7 and Cu-9 catalysts. These spectra have been acquired at similar NO pressures (~0.6 mbar). (B) Relationship between the catalytic activity at 350°C for the SCR of NOx and the IR-NO area associated to Cu<sup>2+</sup> species (1910+1898 cm<sup>-1</sup>) for fresh and steamed at 750°C SAPO34-7 and Cu-9 catalysts.**



**Table 1: Molar ratios used for the synthesis of each Cu-SAPO-34**

<b>Sample</b>	<b>P/Al</b>	<b>Si/Al</b>	<b>Si/(Al+P)</b>	<b>Cu-TEPA/(Al+P)</b>	<b>DEA/(Al+P)</b>	<b>TEA/(Al+P)<sup>e</sup></b>
<b>SAPO34-8</b>	0.8	0.36	0.2	0.1	0.4	---
<b>SAPO34-7</b>	0.8	0.36	0.2	0.05	0.45	---
<b>Cu-1</b>	0.9	0.19	0.1	0.05	0.45	---
<b>Cu-2</b>	0.9	0.19	0.1	0.025	0.475	---
<b>Cu-3</b>	0.8	0.2	0.11	0.05	0.45	---
<b>Cu-4</b>	0.8	0.2	0.11	0.025	0.475	---
<b>Cu-5</b>	0.75	0.25	0.143	0.05	0.45	---
<b>Cu-6</b>	0.75	0.25	0.143	0.025	0.475	---
<b>Cu-7</b>	0.7	0.3	0.176	0.05	0.45	---
<b>Cu-8</b>	0.7	0.3	0.176	0.025	0.475	---
<b>Cu-9</b>	0.7	0.3	0.176	0.05	0.15	0.3

<sup>a</sup> All materials were prepared with  $H_2O/(Al+P) = 10$  and 5%wt of SAPO-34 crystals as seeding;

<sup>b</sup> All materials were crystallized at 150°C for 5 days; <sup>c</sup> Cu-tetraethylenepentamine; <sup>d</sup> diethylamine; <sup>e</sup> tetraethylammonium

**Table 2: Chemical analyses and solid yields for the synthesized Cu-SAPO-34 materials**

Sample	Si/TO <sub>2</sub>	Cu/TO <sub>2</sub>	%wt Cu	Cu/cavity	Solid yield (%wt)
SAPO34-8	0.180	0.054	6.1	1.1	~90
Cu-1	0.106	0.062	6.6	1.1	~88
Cu-2	0.106	0.051	5.4	1.0	~40
Cu-3	0.104	0.059	6.2	1.0	~85
Cu-4	0.109	0.049	5.2	0.9	~46
Cu-5	0.112	0.058	6.1	1.0	~87
Cu-6	N.D. <sup>d</sup>	N.D.	N.D.	N.D.	~46
Cu-7	0.122	0.057	6.0	1.0	~86
Cu-8	N.D.	N.D.	N.D.	N.D.	~40
Cu-9	0.141	0.031	3.3	0.6	~94

<sup>a</sup> Cu atoms per CHA unit cell (each CHA unit cell has 36 T atoms); <sup>b</sup> Cu atoms per CHA cavity (each CHA unit cell has 2 cavities); <sup>c</sup> calculated as %wt of the oxides introduced in the synthesis gel; <sup>d</sup> N.D.: not determined.

**Table 3: Elemental analyses de Cu-2 and Cu-9**

<b>Sample</b>	<b>%wt N</b>	<b>%wt C</b>	<b>C/N)<sub>real</sub></b>	<b>%TEPA</b>	<b>%DEA</b>
<b>Cu-1</b>	5.1	9.3	2.1	79	21
<b>Cu-2</b>	4.6	8.9	2.2	75	25
<b>Cu-9</b>	3.2	9.3	3.4	---	---

## References:

- 
- [1] a) M. Moliner, C. Martinez, A. Corma, *Chem. Mater.* **2013**, *In Press*; b) I. Bull, R. S. Boorse, W. M. Jaglowski, G. S. Koermer, A. Moini, J. A. Patchett, W. M. Xue, P. Burk, J. C. Dettling, M. T. Caudle, *U.S. Patent 0,226,545*, **2008**; c) J. H. Kwak, R. G. Tonkyn, D. H. Kim, J. Szanyi, C. H. F. Peden, *J. Catal.* **2010**, *275*, 187; d) S. T. Korhonen, D. W. Fickel, R. F. Lobo, B. M. Weckhuysen, A. M. Beale, *Chem. Commun.* **2011**, *47*, 800; e) M. Moliner, C. Franch, A. E. Palomares, M. Grill, A. Corma, *Chem. Commun.* **2012**, *48*, 8264.
- [2] a) J. H. Kwak, H. Zhu, J. H. Lee, C. H. F. Peden, J. Szanyi, *Chem. Commun.* **2012**, *48*, 4758; b) J. H. Kwak, D. Tran, J. Szanyi, C. H. F. Peden, J. H. Lee, *Catal. Lett.* **2012**, *142*, 295.
- [3] B. Z. Zhan, E. Iglesia, *Angew. Chem., Int. Ed.* **2007**, *46*, 3697.
- [4] a) L. Ren, L. Zhu, C. Yang, Y. Chen, Q. Sun, H. Zhang, C. Li, F. Nawaz, X. Meng, F. S. Xiao, *Chem. Commun.* **2011**, *47*, 9783; b) R. Martínez-Franco, M. Moliner, C. Franch, A. Kustov, A. Corma, *Appl. Catal. B* **2012**, *127*, 273.
- [5] M. Moliner, *ISRN Materials Science*, **2012**, Article ID 789525.
- [6] a) N. Trukhan, U. Mueller, I. Bull, *U.S. Patent 2011/0076229*, **2011**; b) R. Martínez-Franco, M. Moliner, J. R. Thogersen, A. Corma, *ChemCatChem*. **2013**, *5*, 3316.
- [7] a) I. Bull, U. Muller, *US2010/0310440A1*, **2010**; b) U. Deka, I. Lezcano-Gonzalez, S. J. Warrender, A. L. Picone, P. A. Wright, B. M. Weckhuysen, A. M. Beale, *Micropor. Mesopor. Mater.* **2013**, *166*, 144.
- [8] G. T. Palomino, P. Fiscaro, S. Bordiga, A. Zecchina, E. Giamello, C. Lamberti, *J. Phys. Chem. B* **2000**, *104*, 4064.
- [9] J. H. Baik, S. D. Yim, I.-S. Nam, Y. S. Mok, J.-H. Lee, B. K. Cho, S. H. Oh, *Top. Catal.* **2004**, *30–31*, 37.
- [10] J. Chen, P. A. Wright, J. M. Thomas, S. Natarajan, L. Marchese, S. M. Bradley, G. Sankar, C. R. A. Catlow, P. L. Gai-Boyes, *J. Phys. Chem.* **1994**, *98*, 10216.
- [11] R. Vomscheid, M. Briend, M. J. Peltre, P. P. Man, D. Barthomeu, *J. Phys. Chem.* **1994**, *98*, 9614.
- [12] J. Wang, T. Yu, X. Wang, G. Qi, J. Xue, M. Shen, W. Li, *Appl. Catal. B.* **2012**, *127*, 137.
- [13] a) Y. Wan, J. Ma, Z. Wang, W. Zhou, S. Kaliaguine, *J. Catal.* **2004**, *227*, 242; b) A. Sultana, T. Nanba, M. Haeda, M. Sasaki, H. Hamada, *Appl. Catal. B.* **2010**, *101*, 61.
- [14] M. Richter, M. J. G. Fait, R. Eckelt, *Appl. Catal. B.* **2007**, *73*, 269.
- [15] P. N. R. Vennestrøm, A. Katerinopoulou, R. R. Tiruvalam, A. Kustov, P. G. Moses, P. Concepcion, A. Corma, *ACS Catal.* **2013**, *3*, 2158.
- [16] a) R. Kefirov, A. Pentoka, K. Hadjiivanov, S. Dzwigaj, M. Che, *Micropor. Mesopor. Mater.* **2008**, *116*, 180; b) Y. Fu, Y. Tian, P. Lin, *J. Catal.* **1991**, *132*, 85; c) K. Hadjiivanov, H. Knozinger, *Phys. Chem. Chem. Phys.* **2001**, *3*, 1132.
- [17] K. Hadjiivanov, *Catal. Rev. Sci. Eng.* **2000**, *42*, 71.
- [18] a) D. B. Akolekar, S. K. Bhargava, *Appl. Catal. A* **2011**, *207*, 355; b) A. Franche, E. Gianotti, L. Marchese, *Catal. Today* **2003**, *77*, 371; c) K. I. Hadjiivanov, M. M. Kantcheva, D. G. Klissurski, *J. Chem. Soc, Faraday Trans.* **1996**, *92*, 4595.
- [19] F. Giordanino, P. N. R. Vennestrom, L. F. Lundegaard, F. N. Stappen, S. Mossin, P. Beato, S. Bordiga, C. Lamberti, *Dalton Transactions*, **2013**, *4*, 12741.
- [20] D. B. Akolekar, S. K. Bhargava, K. Fogar, *J. Chem. Soc, Faraday Trans.* **1998**, *94*, 155.